Electronic Supplementary Information

Immobilizing ultrasmall Pt nanocrystals onto 3D interweaving BCN nanosheet-graphene networks enables efficient methanol oxidation reaction

Binfeng Shen, Yujie Wei, Pengyun Sun, Haiyan He, Guobing Ying,* Huajie Huang *

College of Mechanics and Materials, Hohai University, Nanjing 210098, China

*E-mail: yinggb2010@126.com or huanghuajie@hhu.edu.cn

Supplementary Results:

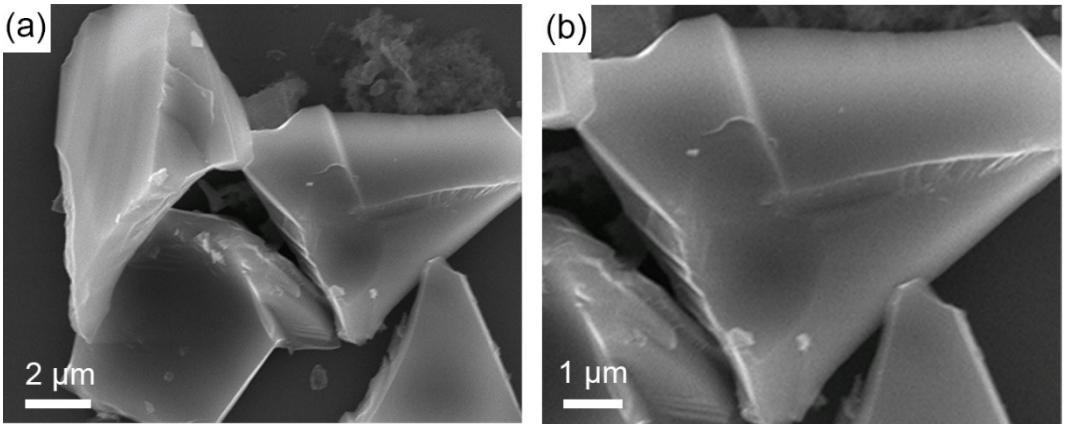

Fig. S1 Typical FE-SEM images of the bulk g-C_3N_4 powder at different magnifications.

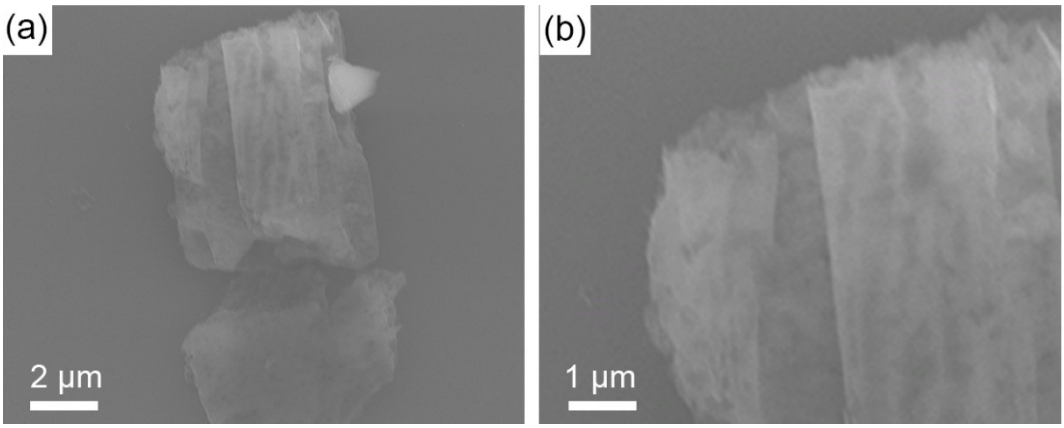

Fig. S2 Typical FE-SEM images of the exfoliated g-C_3N_4 nanosheets at different magnifications.

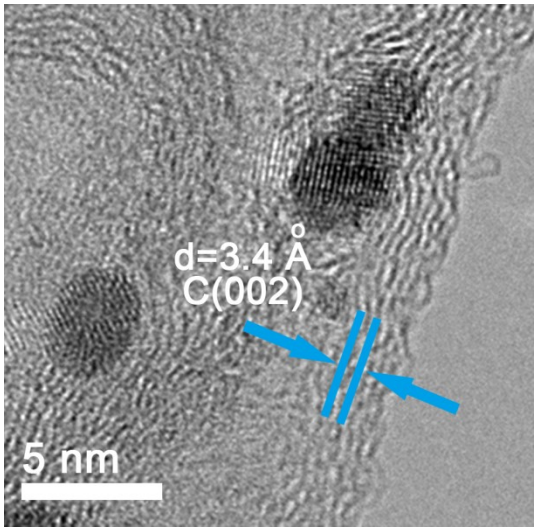

Fig. S3 HR-TEM image of the 3D Pt/BCN-G nanoarchitecture shows the lattice fringes of graphene nanosheets.

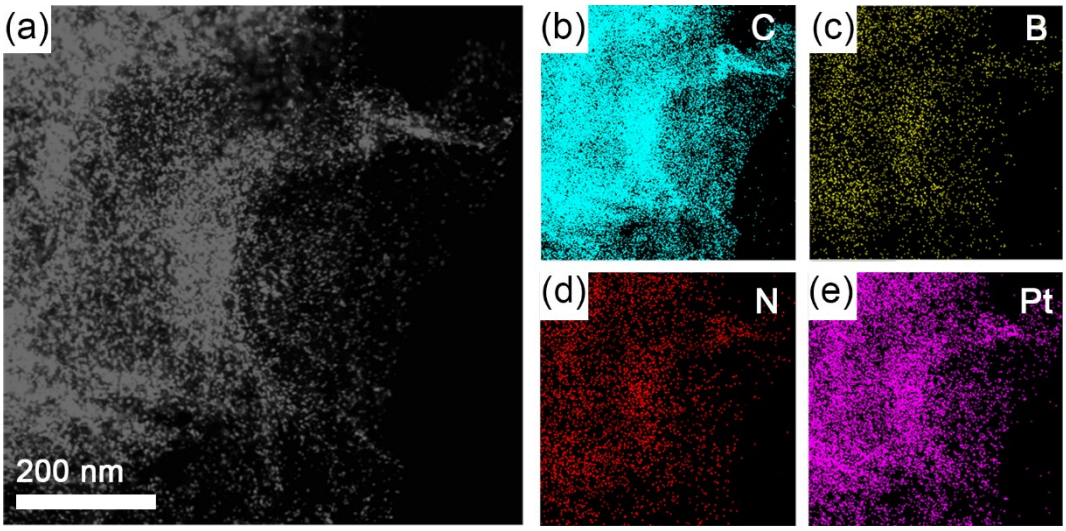

Fig. S4 (a) Low-magnification HAADF-STEM and the corresponding elemental mapping images reveal the homogeneous dispersion of (b) C, (c) B, (d) N and (e) Pt elements in the Pt/BCN-G nanoarchitecture.

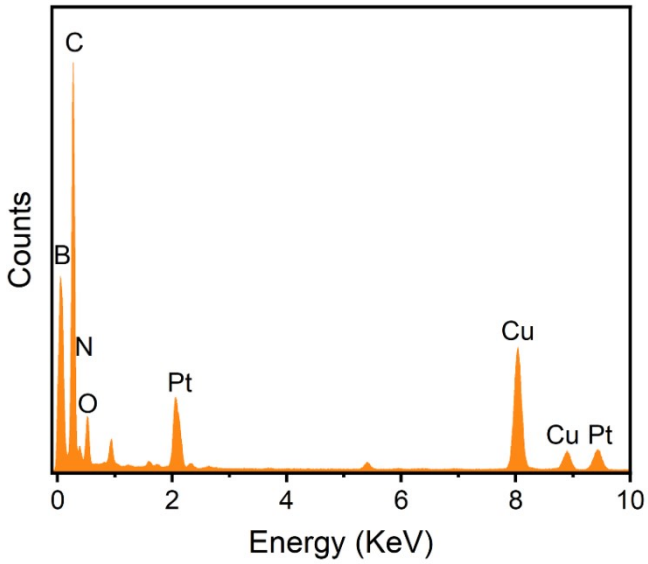

Fig. S5 EDX spectrum of the 3D Pt/BCN-G nanoarchitecture verifies the presence of C, B, N and Pt components in the hybrid.

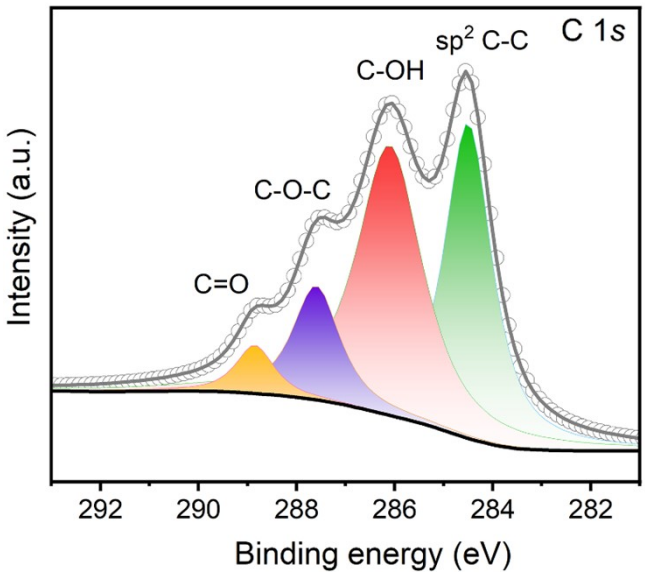

Fig. S6 High-resolution C 1s XPS spectrum of GO, indicating that the carbon sheets possess a large number of oxygen functional groups.

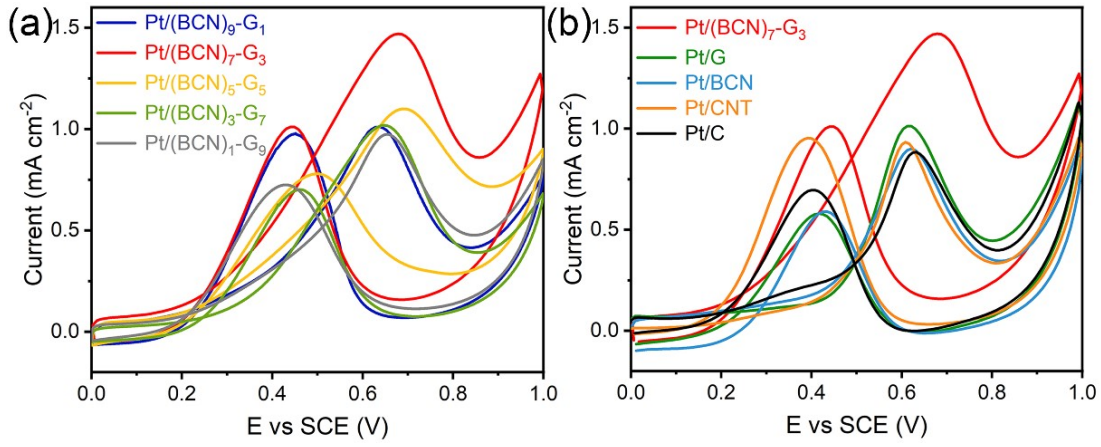

Fig. S7 The ECSA-normalized CV curves of (a) the Pt/BCN-G electrodes with different BCN/G ratios, and (b) Pt/$(BCN)_7$-G_3, Pt/G, Pt/BCN, Pt/CNT, and Pt/C electrodes in 0.5 M H_2SO_4 and 1 M CH_3OH solution at 50 mV s^{-1}.

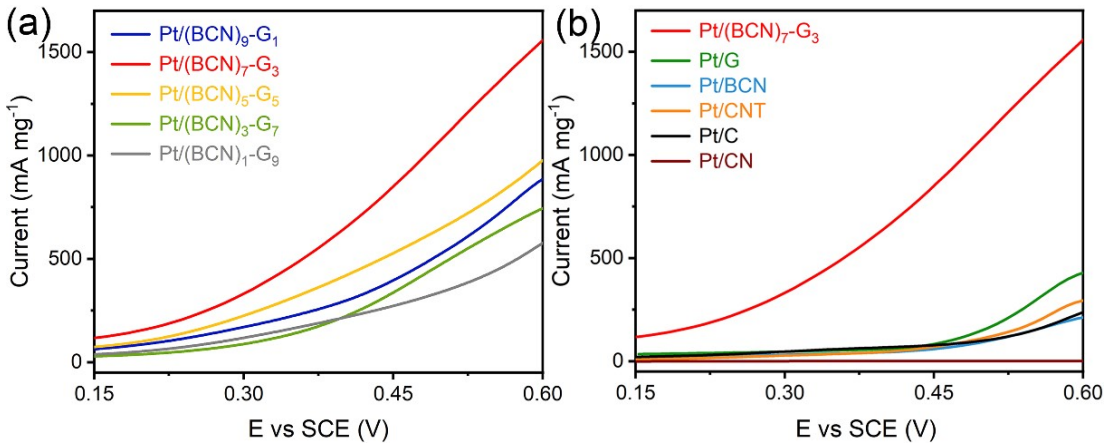

Fig. S8 (a) LSV curves of (a) the Pt/BCN-G electrodes with different BCN/G ratios and (b) Pt/$(BCN)_7$-G_3, Pt/G, Pt/BCN, Pt/CNT, Pt/C and Pt/CN electrodes in 0.5 M H_2SO_4 and 1 M CH_3OH solution at 50 mV s^{-1}.

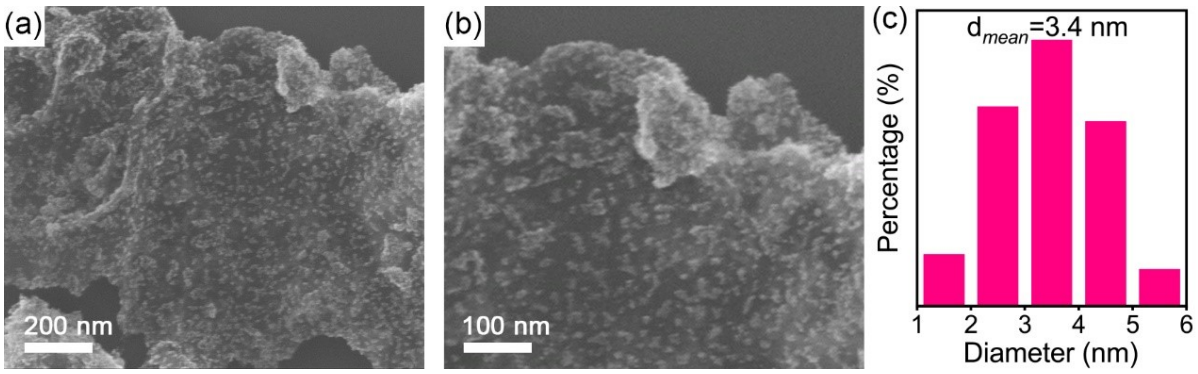

Fig. S9 (a-b) FE-SEM images and (c) corresponding Pt size distribution of the Pt/BCN-G catalyst after the long-term stability test.

Table S1 The B and N contents in various Pt/BCN-G catalysts.

Catalyst	B (at%)	N (at%)
$Pt/(BCN)_1$-G_9	1.0	2.6
$Pt/(BCN)_3$-G_7	1.7	7.7
$Pt/(BCN)_5$-G_5	4.8	12.8
$Pt/(BCN)_7$-G_3	6.6	18.0
$Pt/(BCN)_9$-G_1	8.5	23.2

Table S2 Compiled study comparing CV results for different catalysts.

Electrode	ECSA ($m^2 g^{-1}$)	Mass activity ($mA mg^{-1}$)	Specific activity ($mA cm^{-2}$)
$Pt/(BCN)_1$-G_9	69.9	680.1	0.97
$Pt/(BCN)_3$-G_7	79.2	806.5	1.02
$Pt/(BCN)_5$-G_5	110.4	1213.5	1.10
$Pt/(BCN)_7$-G_3	121.2	1782.2	1.47
$Pt/(BCN)_9$-G_1	93.6	946.3	1.01
Pt/G	43.3	438.5	1.01
Pt/BCN	24.6	221.5	0.9
Pt/CNT	31.9	297.7	0.93
Pt/C	29.7	262.5	0.88

Table S3 Comparison of methanol oxidation behavior of the 3D $Pt/(BCN)_7$-G_3 catalyst with various state-of-the-art Pt-based electrocatalysts.

Electrode	ECSA ($m^2 g^{-1}$)	Mass activity ($mA mg^{-1}$)	Electrolyte	Ref.
$Pt/(BCN)_7$-G_3	121.2	1782.2	0.5 M H_2SO_4 +1 M CH_3OH	This work
Pt/[BMIM]BF_4/CNT	N. A	155.0	0.5 M H_2SO_4 +1 M CH_3OH	[48]
Pt/imidazolium-salt/CNT	67.6	410.0	0.5 M H_2SO_4 +0.5 M CH_3OH	[22]
Pt/N-doped graphene	N. A	376.2	0.5 M H_2SO_4 +0.5M CH_3OH	[49]
Pt/RGO-$Ti_3C_2T_x$	90.1	1102.0	0.5 M H_2SO_4 +1 M CH_3OH	[37]
Pt/RGO/CNT	117.3	691.1	0.5 M H_2SO_4 +1 M CH_3OH	[50]
Pt/G-C_3N_4	69.0	621.8	0.5 M H_2SO_4 +1 M CH_3OH	[39]
Pt/RGO-MoS_2	104.3	737.8	0.5 M H_2SO_4 +1 M CH_3OH	[51]
PtPd dendrites/RGO	81.6	647.2	0.5 M H_2SO_4 +1 M CH_3OH	[52]